Morphological insights into the mechanism of catalytic aquathermolysis of crude oil with an easily prepared high-efficiency Fe_3O_4-containing catalyst

Dong Lin[1], Huihong Zhu[2], Yining Wu[3], Yibin Liu[1], Xiaobo Chen[1], Chong Peng[2,*], Chaohe Yang[1], Xiang Feng[1,*]

[1]*State Key Laboratory of Heavy Oil Processing, China University of Petroleum, Qingdao 266580,China*

[2]*Dalian Research Institute of Petroleum and Petrochemicals, SINOPEC, Dalian 116045, China*

[3]*College of Petroleum Engineering, China University of Petroleum, Qingdao 266580, China*

Abstract: Elucidating the underlying structure-performance relationship of Fe_3O_4-containing catalysts for the aquathermolysis of crude oil is essential for the design of efficient heterogeneous catalysts. Therefore, recyclable Fe_3O_4 nanoparticles (NPs) with different morphology and particle size were first prepared and tested for catalytic aquathermolysis. The easily prepared Fe_3O_4 NPs with irregular morphology (L-Fe_3O_4) have larger intercrystalline mesopores than oleic acid-modified Fe_3O_4 NPs. This leads to enhanced mass transfer ability, more accessible active sites and thus better aquathermolysis performance. Moreover, these L-Fe_3O_4 NPs were loaded on a heulandite support by a scalable co-precipitation method, and this L-Fe_3O_4/heulandite catalyst showed very good performance in catalytic aquathermolysis, with a viscosity decrease of extra-heavy crude oil of 85.0%. The underlying structure-performance

relationship was systematically investigated by XRD, HRTEM, EDX-mapping, FT-IR, elemental analysis, SARA (saturate, aromatic, resin and asphaltene) analysis and ^{1}H NMR. The Fe_3O_4/heulandite catalyst broke C-S bonds and reduced the resin and asphaltene content of the oil. This work is important for the design of Fe_3O_4-containing catalysts in catalytic aquathermolysis.

Keywords: heavy oil, aquathermolysis, mechanism, preparation method, Fe_3O_4/heulandite.

1. Introduction

Worldwide crude oil reserves cannot meet the increasing huge demands due to the rapid development of economy but limited oil resources [1, 2]. In order to deal with this issue, abundant heavy oil is attracting worldwide attention [3, 4]. However, heavy oil has high viscosity, causing high costs and difficulties in exploitation and transportation. Hence, different technologies such as chemical, thermal and microbial recovery were developed to handle this problem [5, 6]. One of the most popular and effective ways to recover oil from crude oil is aquathermolysis [7, 8]. In 1982, Hyne et al. studied the interaction between steam and heavy oil and described the chemical reactions that occur as "aquathermolysis" [9]. Later Clark et al. found that steam injected into crude oil cannot only decrease the viscosity of the crude oil but also slightly improved its quality [10-14]. However, further research showed that these changes happening at the beginning of aquathermolysis are strongly suppressed in the presence of heteroatoms (i.e., S, N, O). That is because the heteroatoms in the crude oil react with other chemical groups to form large molecules by van der Waals forces or hydrogen bonds [15], and this polymerization can cause regression. In order to deal with these problems [16-19], high temperature steam was injected into the crude oil with the addition of catalysts, which can effectively reduce the viscosity of crude oil and terminate polymerization during the early reaction period [20, 21]. Apparently, the catalyst plays a crucial role in the catalytic aquthermolysis for effectively reducing viscosity [22]. Therefore, a high-efficiency and easily recyclable catalyst is the key for catalytic aquathermolysis.

In recent years, heterogeneous nickel-based, iron-based and cobalt-based

nanocatalysts showed enhanced performance for catalytic aquathermolysis [23, 24]. Compared with homogeneous catalysts, heterogeneous catalysts can more easily be recycled and reused. Iron-based catalysts are not only cheap but also environmentally friendly and, therefore, seem promising in the industrial application in catalytic aquathermolysis [25]. Chen et al. found that α-Fe_2O_3 synthesized by mixing aromatic sulfonic acid with Fe_2O_3 reduces the viscosity (i.e., 93.3%) [19]. Nugraha et al. showed that Fe_3O_4 prepared by microwave-assisted co-precipitation reduced the viscosity by 30% [26]. Nurhayati et al. deposited α-Fe_2O_3 on a zeolite by microwave-assisted co-precipitation and found that the catalyst exhibited a strong ability for reducing viscosity (i.e., 89%) [27]. In our previous study, we found that the synergy between a metal oxide and carrier in catalytic aquathermolysis is favorable for reducing viscosity [28]. Although Fe-based catalysts have attracted much attention, up to now limited attention has been paid to their structure-performance relationship for catalytic aquathermolysis and the underlying mechanism.

In this paper, Fe_3O_4 nanoparticles with different morphology were synthesized, and their intrinsic structure-performance relationships were investigated by XRD, HRTEM, EDX-mapping, FT-IR, elemental analysis, SARA (saturate, aromatic, resin, asphaltene) analysis and ^{1}H NMR. We found that simply reducing the size of Fe_3O_4 nanoparticles did not enhance the performance of catalytic aquathermolysis. However, the larger average pore diameter significantly increased viscosity reduction of crude oil in catalytic aquathermolysis. A designed Fe_3O_4/heulandite catalyst showed enhanced performance, with a viscosity reduction of 85.0%. The Fe_3O_4-containing catalyst plays

a key role in reducing the viscosity by breaking C-S bonds and decreasing the resin and asphaltene content in the crude oil. This paper sheds new light on the design of Fe_3O_4-containing catalyst for catalytic aquathermolysis.

2. Experimental

2.1 Synthesis of Fe_3O_4 nanoparticles

Fe_3O_4 nanoparticles were synthesized by two different co-precipitation methods. One was used to synthesize large Fe_3O_4 nanoparticles and the other to synthesize small Fe_3O_4 nanoparticles. The catalysts were denoted as L- Fe_3O_4 or S- Fe_3O_4, respectively.

L-Fe_3O_4 nanoparticles were synthesized by adding 3.70 g $FeCl_3$ (AR, ShangHai Hushi Laboratorial Equipment Co., Ltd) and 3.17 g $Fe_2SO_4 \cdot 7H_2O$ (AR, ShangHai Hushi Laboratorial Equipment Co., Ltd) to 100 ml deionized water. Then 0.5 M NaOH (AR, ShangHai Hushi Laboratorial Equipment Co., Ltd) solution was added dropwise to the above solution (with Fe^{3+} and Fe^{2+} ions in the ratio of 2:1) until the pH reached the value of 10, and the slurry was stirred for 0.5 h at room temperature. The resulting L-Fe_3O_4 nanoparticles were separated by magnetic separation and washed three times with deionized water. The resulting catalyst was dried at 50 ^{o}C.

S-Fe_3O_4 nanoparticles were synthesized by mixing 10.80 g $FeCl_3 \cdot 6H_2O$ (AR, ShangHai Hushi Laboratorial Equipment Co., Ltd) and 4.98 g $FeCl_2 \cdot 4H_2O$ (AR, ShangHai Hushi Laboratorial Equipment Co., Ltd) with 25 ml deionized water. Afterwards, 0.2 g NaOH and 10 g NaOH were put into 50 ml and 250 ml deionized water respectively. The solution containing 0.2 g NaOH was stirred at 65 ^{o}C.

Subsequently the iron-containing solution and the solution containing 10 g NaOH were added dropwise to the solution containing 0.2 g NaOH under stirring at 65 °C. When the black composite was formed, 0.835 g oleic acid (AR, ShangHai Hushi Laboratorial Equipment Co., Ltd) was added to the mixture. The resulting S-Fe_3O_4 nanoparticles were washed with deionized water and ethanol, and then the black nanoparticles were separated by a magnetic field and dried at 50 °C.

2.2 Synthesis of Fe_3O_4/heulandite catalysts

A Fe_3O_4/heulandite catalyst was prepared by adding 4.00 g of milled heulandite zeolite into 100 ml deionized water and continuously stirring for 0.5 h. After that, 3.17 g $Fe_2SO_4 \cdot 7H_2O$ (AR, ShangHai Hushi Laboratorial Equipment Co., Ltd) and 3.70 g $FeCl_3$ (AR, ShangHai Hushi Laboratorial Equipment Co., Ltd) were dissolved in deionized water under stirring at room temperature. Afterwards, 100 ml of this solution, containing Fe^{2+} and Fe^{3+} ions in the ratio of 1:2, was added to the slurry of heulandite in water. The mixture was heated at 80 °C under vigorous stirring for 6 h, followed by dropwise addition of 0.5 M NaOH until the pH reached 10. The as-synthesized black composite was magnetically separated and dried at 50 °C.

2.3 Catalytic aquathermolysis of crude oil

Two kinds of oil were used in the catalytic aquathermolysis, which are from the Shengli oil field (extra-heavy oil) and Xinjiang oil field (light oil), both from China. In all aquathermolysis experiments, 2.5 g of catalyst was mixed with 10 g of deionized water, and the resulting slurry was added to 40 g of oil in an autoclave. The autoclave

was kept at 3 MPa under N_2 atmosphere and was heated to 280 °C under intense agitation for 6 h. Then the oil sample was cooled down and taken out for further analysis. The low viscosity of the Xinjiang oil was measured by a reverse flow type viscometer at 50 °C and the high viscosity of Shengli oil was recorded by a BROOKFIELD DV-II+PRO instrument at 50 °C. The viscosity reduction (△η%) was calculated as follows: $\triangle\eta\% = (\eta_0 - \eta)/\eta_0$ where η_0 (mm^2/s or cp) and η (mm^2/s or cp) are the viscosities of the oil before and after the catalytic aquathermolysis, respectively.

2.4 Characterizations of catalysts and oil

The crystal phases of the Fe_3O_4 nanoparticles were characterized by X-ray diffraction (XRD, X'pert PRO MPD, Cu K_α radiation) with a scan speed of 10°/min. The morphology and size of the iron oxide nanoparticles were observed with a Transmission Electron Microscope (TEM, JEM-2100UHR). The nitrogen adsorption-desorption isotherms were determined with a volumetric adsorption analyzer (Micromeritics 3-Flex 3500). Elements of oil before and after catalytic aquathermolysis were measured by elemental analysis (EL, Vario ELIII). Infrared spectra of the oil samples were recorded on a Nicolet NEXUS 670 Fourier-transform (FT-IR) spectrometer with air as background. The contents of the saturated hydrocarbon, aromatic hydrocarbon, resin and asphaltene components of the oil were obtained by the SARA method according to the industrial standard NB/SH/T 0509-2010. The oil samples were characterized by ^1H nuclear magnetic resonance (^1H-NMR, BRUKER-AM300) using $CDCl_3$ as the solvent.

3. Results and Discussion

3.1 Characterization of the Fe_3O_4 nanoparticles

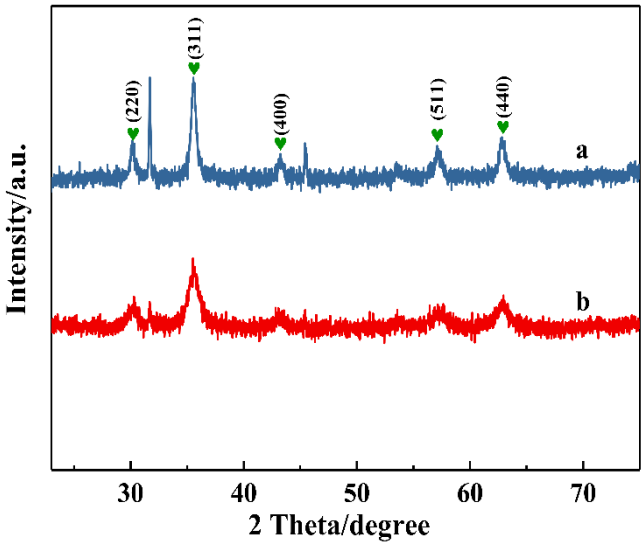

Figure 1. XRD spectra of L-Fe_3O_4 nanoparticles (a) and S-Fe_3O_4 nanoparticles (b).

Figure 1 shows the XRD patterns of the L-Fe_3O_4 nanoparticles and S-Fe_3O_4 nanoparticles. The black catalyst is magnetic, indicating that magnetite may be the dominant crystal structure although the phase of maghemite might be included in the catalyst [29]. The XRD peaks of Fe_3O_4 at 30.14 °, 35.55 °, 43.29 °, 57.08 ° and 62.73 ° correspond to the (220), (311), (400), (511) and (440) reflections of Fe_3O_4 respectively, confirming the successful synthesis of Fe_3O_4 nanoparticles, with face-centered cubic (fcc) structure [30]. The sharp lines at 31.20 ° and 45.93 ° may correspond to the (003), (620) reflections of Fe_2O_3 respectively. The (311) peak of S-Fe_3O_4 nanoparticles is broader than that of L-Fe_3O_4 nanoparticles confirming that the size of the S-Fe_3O_4 nanoparticles is smaller [29, 31]. The size of the Fe_3O_4 nanoparticles can be calculated with the Debye Scherrer formula:

$$D = \frac{K\lambda}{\beta \cos\theta} \quad (1)$$

where D is the size of the Fe_3O_4 nanoparticles, K is the Scherrer constant (0.89), λ is the wave length of the X-rays (0.154 nm), β is the full width at half maximum, and θ is the reflection angle (17.775 ^{o}). Thus the average sizes of the L-Fe_3O_4 and S-Fe_3O_4 particles are 14.1 and 7.4 nm, respectively. The smaller size of the S-Fe_3O_4 nanoparticles is attributed to the use of oleic acid, which reduces the agglomeration of Fe_3O_4 particles [32].

The morphology, size distribution and exposed crystal planes of Fe_3O_4 nanoparticles were characterized by TEM and HRTEM. Figures 2 (a) and (b) show typical TEM images of S-Fe_3O_4 and L-Fe_3O_4 nanoparticles, respectively. The S-Fe_3O_4 nanoparticles have a regular shape while the L-Fe_3O_4 nanoparticles are more irregular in morphology. More than 150 Fe_3O_4 nanoparticles were selected to calculate the mean size and size distribution of the Fe_3O_4 nanoparticles. The column diagrams show that the mean size of the S-Fe_3O_4 and L-Fe_3O_4 nanoparticles is 5.8 and 18.5 nm respectively, which is in reasonable agreement with the result of the Debye Scherrer formula. The HRTEM images were used to show the crystal planes, which usually have different surface energy. Figure 2 (c-h) shows that the crystal planes are (220), (111), (400) and (311). Furthermore, the observed crystal planes are almost the same for the S-Fe_3O_4 and L-Fe_3O_4 nanoparticles according to the SAED patterns shown in Figure 2 (i) and (j).

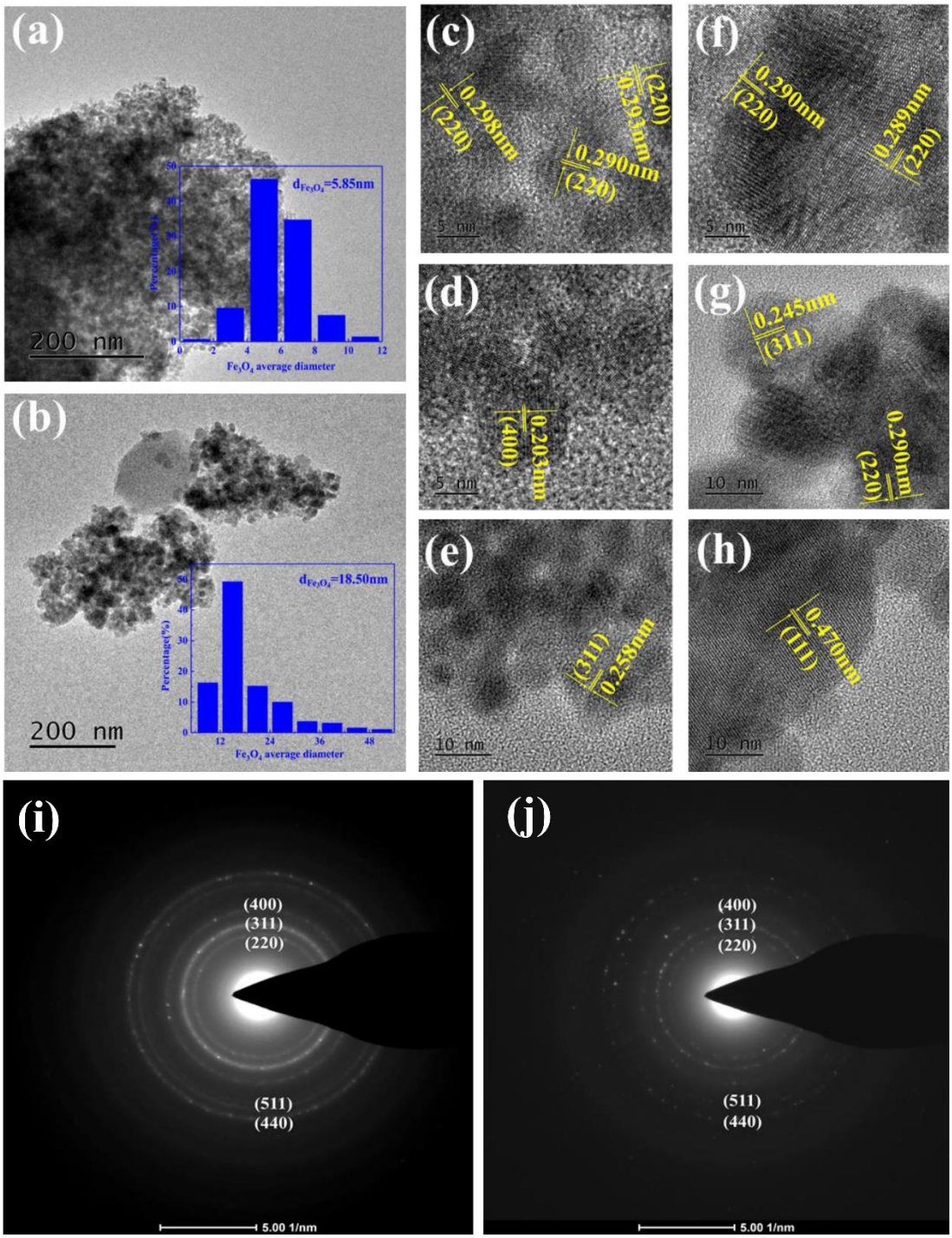

Figure 2. Typical TEM (a, b) and HRTEM (c, d, e, f, g, h) images of S-Fe_3O_4 nanoparticles (a, c, d, e) and L-Fe_3O_4 nanoparticles (b, f, g, h). Selected-area electron diffraction (SAED) patterns of S-Fe_3O_4 nanoparticles (i) and L-Fe_3O_4 nanoparticles (j). The insets show the size distribution of the Fe_3O_4 nanoparticles.

Figure 3 shows the N_2 adsorption/desorption isotherms and pore size distributions of the S-Fe_3O_4 and L-Fe_3O_4 nanoparticles. They exhibit the typical type IV adsorption-desorption isotherms with the hysteresis loops due to the capillary condensation indicating the presence of mesopores in the S-Fe_3O_4 and L-Fe_3O_4 nanoparticles. The structural properties of the S-Fe_3O_4 and L-Fe_3O_4 nanoparticles are given in Table 1. The surface area of the L-Fe_3O_4 nanoparticles (i.e., 50.8 m^2/g) is similar to that of the S-Fe_3O_4 nanoparticles (i.e., 54.9 m^2/g). In addition, the volumes of the mesopores of the S-Fe_3O_4 and L-Fe_3O_4 nanoparticles are almost the same. The average pore diameter of S-Fe_3O_4 is 7.1 nm, smaller than that of 11.0 nm for L-Fe_3O_4. Combining the HRTEM images and BET results, the L-Fe_3O_4 nanoparticles prepared without the addition of oleic acid have a more irregular particle size, leading to larger intercrystalline mesopores. This enhances the mass transfer ability and provides more opportunities for crude oil to contact active sites of L-Fe_3O_4 in the catalytic aquathermolysis.

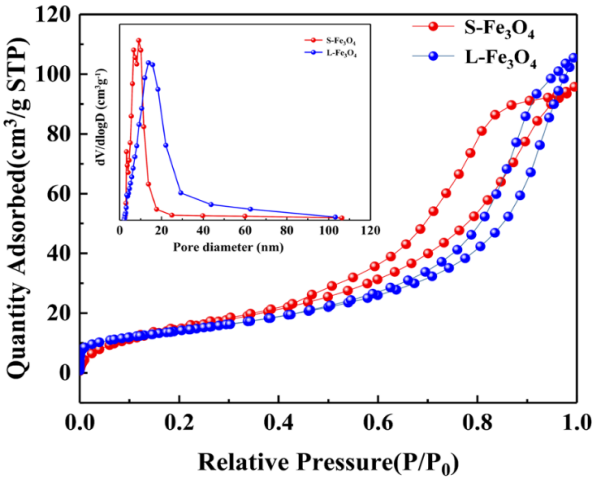

Figure 3. Nitrogen adsorption-desorption isotherms of S-Fe_3O_4 and L-Fe_3O_4 nanoparticles. The inset shows the pore size distributions.

Table 1 Structural properties of Fe_3O_4 nanoparticles prepared by different methods.

Catalyst	S_{BET}[a] (m^2/g)	V_P[b] (cm^3/g)	D_P[c] (nm)
S-Fe_3O_4	54.9	0.15	7.1
L-Fe_3O_4	50.8	0.16	11.0

[a]Specific surface area is based on BET method.

[b]Volume of pores (V_P) is calculated from BJH analysis.

[c]Average pore diameter (D_P) is estimated by desorption isotherm.

3.2 Catalytic aquathermolysis of the Fe_3O_4 nanoparticles catalyst

The viscosity of the light oil before aquathermolysis is 346 mm^2/s and after aquathermolysis with the S-Fe_3O_4 and L-Fe_3O_4 nanoparticles it decreased to 268 and 238 mm^2/s respectively. The performance of the L-Fe_3O_4 nanoparticles was better than that of the S-Fe_3O_4 nanoparticles, indicating that the aquathermolysis is mainly affected by the pore size rather than the particle size, since larger pores expose more accessible surface active sites. The larger pore size originated from the irregular morphology of L-Fe_3O_4 catalyst facilitates the sulfur removal reaction because some of the sulfur-containing compounds have larger size and steric hindrance.

The infrared spectrum of light oil was used to record the changes of functional groups before and after reaction, as shown in Figure 4. It is well known that the absorption peak at 2924 cm^{-1} is due to the C-H stretching of methylene groups and methyl groups [33]. The bands at the 380, 813, 869, 1222 and 1604 cm^{-1} are attributed to polycyclic aromatic hydrocarbons, which become slightly weaker after catalytic

aquathermolysis with the S-Fe_3O_4 and L-Fe_3O_4 nanoparticles due to the broken bonds of the polycyclic aromatic hydrocarbons and hydrogenation of unsaturated groups [33]. The disappearance of the band at 3392 cm^{-1}, which corresponds to hydrogen bonding (i.e., amine and hydroxyl groups), after aquathermolysis with catalyst indicates that Fe_3O_4 can provide additional opportunities for the splitting of hydrogen bonds in the crude oil [34-37].

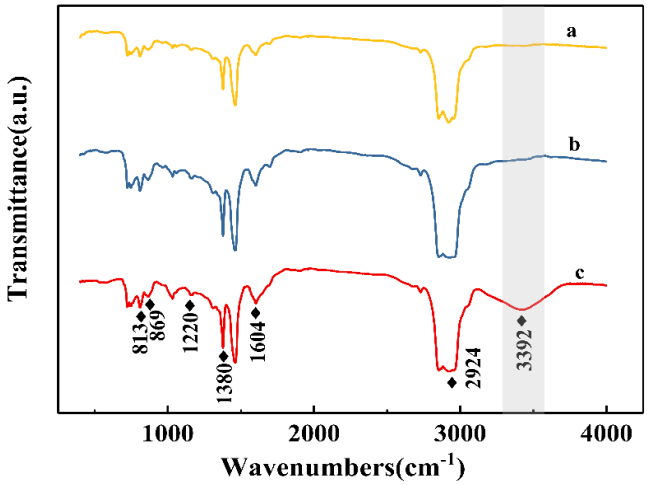

Figure 4 FT-IR Spectra of light oil after aquathermolysis with L-Fe_3O_4 (a), oil after aquathermolysis with S-Fe_3O_4 (b) and crude oil (c).

The changes in the components of the light oil before and after aquathermolysis with Fe_3O_4 nanoparticles are listed in Table 2. The increase of the saturates/aromatics and the decrease of the resin/asphaltene compounds are due to the breaking of chemical bonds and pyrolysis of heavy components, which is in accordance with the changes in viscosity [8]. Compared with the S-Fe_3O_4 catalyst, the L-Fe_3O_4 catalyst results in more saturates/aromatics and less resin/asphaltene compounds. Table 3 shows the elemental analysis results of the oil before and after catalytic aquathermolysis. The H/C molar

ratios after reaction are slightly higher due to the hydrogenation of unsaturated molecules and the breaking of heavy components in the oil. The elemental analysis results are consistent with the results of the viscosity and group compositions. Compared with the crude oil, the S content of the oil after catalytic aquathermolysis with the S-Fe_3O_4 and L-Fe_3O_4 nanoparticles decreased to 4.80 and 4.78% respectively. The decrease of the S content means that S-containing bonds were broken in the aquathermolysis, which is attributed to the addition of the Fe_3O_4 catalyst. Moreover, the sample oil treated with L-Fe_3O_4 had lower S content than that treated with S-Fe_3O_4, and the analysis result is in agreement with the change of viscosity. In order to clearly reveal the effect of the different preparation methods of Fe_3O_4 nanoparticles, Figure 5 is used to show the related influence of morphology during the catalytic aquathermolysis.

Table 2 Group composition of oil samples with different catalysts.

Heavy oil samples	Group composition (%)				
	Saturated HC	Aromatic HC	Resin	Asphaltene	Total
Crude oil	34.6	36.7	15.9	12.8	100
Oil after reaction with S-Fe_3O_4	40.1	37.0	12.8	10.1	100
Oil after reaction with L-Fe_3O_4	39.8	37.9	11.7	10.6	100

Table 3 Elemental analysis of oil after aquathermolysis with different catalysts.

Catalyst	H%	C%	N%	S%	H/C
no	10.8	83.2	0.27	4.94	1.555
S-Fe_3O_4	11.0	83.9	0.27	4.78	1.579
L-Fe_3O_4	11.0	83.6	0.27	4.76	1.584

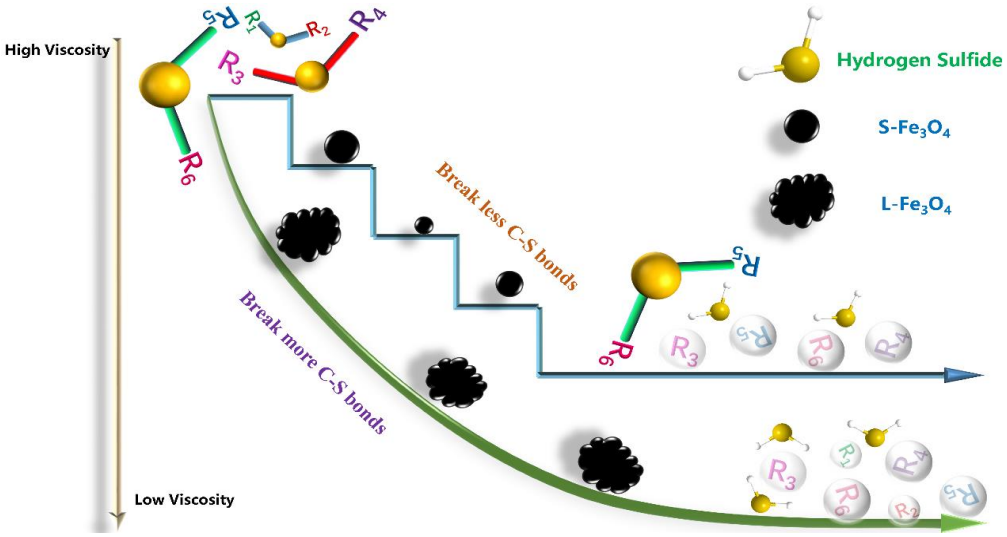

Figure 5 Illustrations of the effect of morphology during aquathermolysis with different Fe_3O_4 nanoparticles

3.3 Catalytic aquathermolysis with the Fe_3O_4/heulandite catalyst

In our previous study, the synergy effect between Fe_3O_4 nanoparticles and carrier was studied and it was found that the carrier can effectively decrease the size of the Fe_3O_4 nanoparticles. It is well known that Fe_3O_4 nanoparticles can easily agglomerate and that oversized magnetic nanoparticles have a negative influence on physical-

chemical properties. In order to disperse the superior Fe_3O_4 nanoparticles more uniformly, the metal oxides were loaded on heulandite by a co-precipitation method.

As Figure 6 shows, Fe_3O_4/heulandite but not heulandite is attracted by a magnetic field. This allows to separate the catalyst by magnetic separation, which is simpler, more efficient and more convenient than traditional high-speed centrifugation [38-40]. Thus, the designed catalyst shows promise for commercial application [41, 42]. Figure 7 shows energy-dispersive X-ray spectroscopy elemental mappings and high-resolution TEM images. Over 150 nanoparticles were selected to calculate the mean size of the Fe_3O_4 nanoparticles. Figure 7 (h) shows that the average size of the Fe_3O_4 nanoparticles deposited on the surface of heulandite is about 15.0 nm. Compared with other co-precipitation methods [43, 44] (25 or 39 nm) and the above-mentioned method (18.5 nm), the size is much smaller benefiting from the synergy effect between support and active component as described in our previous study [28]. The elemental distribution of O, Si, Fe and Al shows that Fe_3O_4 nanoparticles are precipitated uniformly on the external surface of carrier.

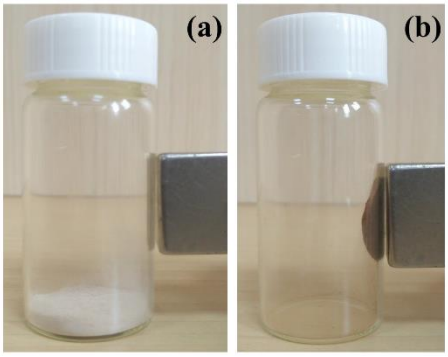

Figure 6. Condition of heulandite (a) and Fe_3O_4/heulandite (b) catalysts in a magnetic field.

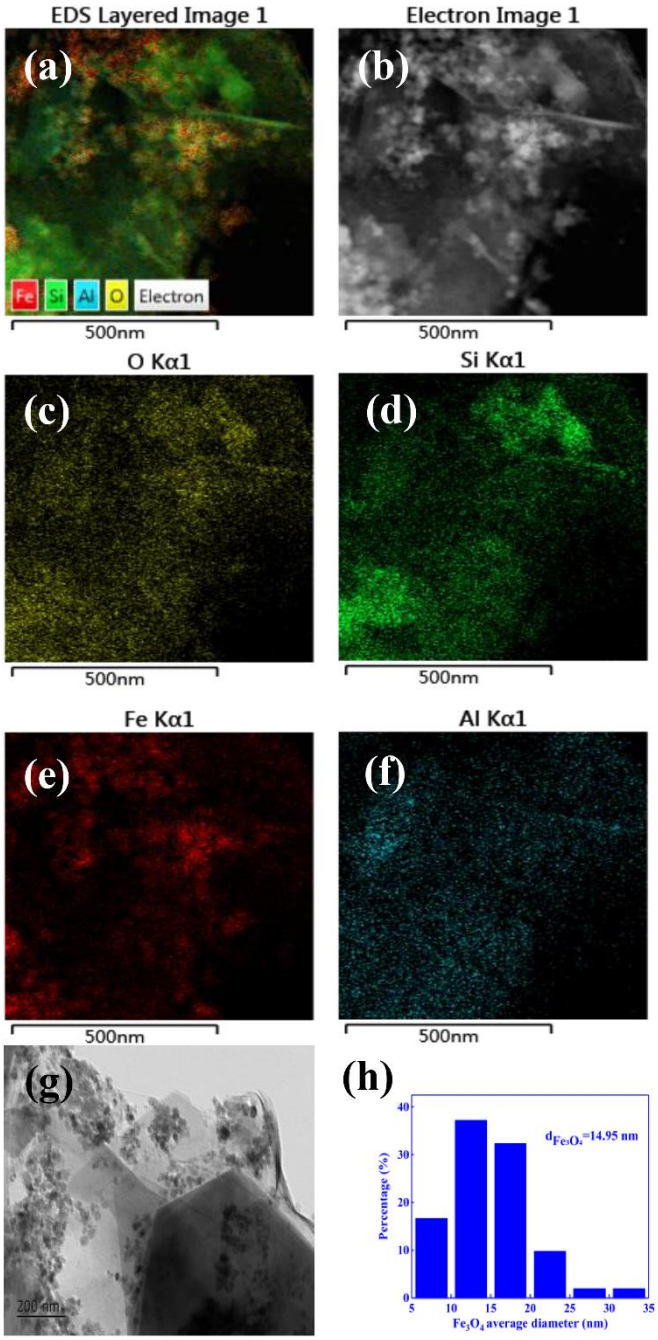

Figure 7. EDX mapping and HRTEM image of the Fe_3O_4/heulandite catalyst.

The viscosity reduction of the extra-heavy crude oil is about 85% after reaction with the designed catalyst, which is a high efficiency. Figure 8 shows the IR spectrum of oil, which can offer information about the distribution of functional groups. As

mentioned above, the peaks at 380, 813, 869, 1222 and 1604 cm^{-1} are assigned to polycyclic aromatic hydrocarbons and the band at 2924 cm^{-1} is attributed to the C-H stretching of methylene groups and methyl groups [33]. All peaks become slightly weaker due to the decomposition of resin and asphaltene in accordance with the significantly reduced viscosity. The intensity of the band at 3392 cm^{-1} decreased strongly due to the high-efficiency activity for breaking some C-R bonds.

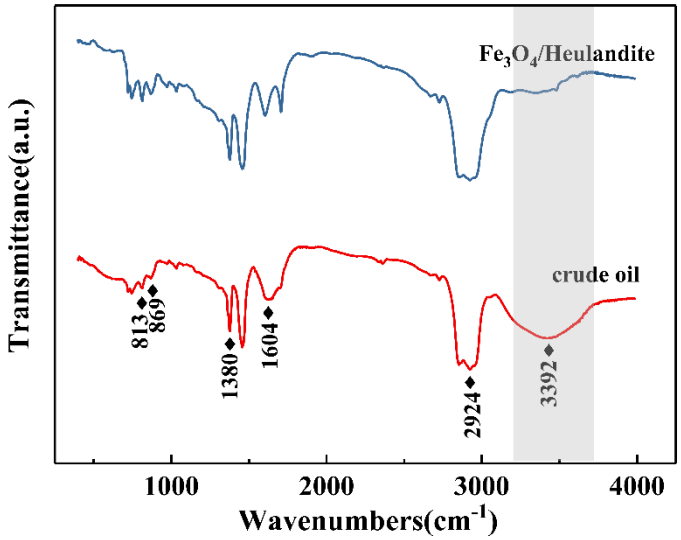

Figure 8 FT-IR Spectra of crude oil and oil after aquathermolysis with Fe_3O_4/heulandite.

Table 4 Group composition of the crude oil before and after treating with Fe_3O_4/heulandite.

Heavy oil samples	Group composition (%)				
	Saturated HC	Aromatic HC	Resin	Asphaltene	Total
Crude oil	45.9	25.3	28.3	0.5	100
Fe_3O_4/heulandite	46.9	27.6	25.4	0.1	100

Table 5 Elemental analysis of oil before and after aquathermolysis with catalyst.

Catalyst	H%	C%	N%	S%	H/C
no	11.6	84.6	0.56	0.47	1.644
Fe_3O_4/heulandite	11.8	85.9	0.56	0.38	1.650

As Table 4 shows, after catalytic aquathermolysis with the Fe_3O_4/heulandite catalyst the fraction of the saturated hydrocarbons and aromatic hydrocarbons of the oil increased from 45.9 and 25.3% to 46.9 and 27.6% respectively, while the resin and asphaltene fraction decreased from 28.3 and 0.5% to 25.4 and 0.1% respectively. The results indicate that the designed magnetic catalyst promotes the pyrolysis of the heavy components of crude oil (e.g., resin and asphaltene) during catalytic aquathermolysis. The changes of the components are in accordance with the variation of viscosity. Table 5 lists the content of the elements (i.e., S, N, C, H) and the H/C ratio before and after reaction with the catalyst. The H/C ratio increased from 1.644 to 1.650. The enhanced performance is ascribed to the hydrogenation of unsaturated groups during aquathermolysis in agreement with the FT-IR results [8]. Importantly, the S content after reaction with catalyst decreased from 0.47 to 0.38% demonstrating that C-S bonds were broken and that S-containing molecules were removed from the crude oil. The N content of the oil after aquathermolysis remained unchanged compared with that of oil before reaction. This result indicates that Fe_3O_4-containing catalyst has almost no influence on C-N bonds, which is widely regarded as the most stable bond in crude oil [25].

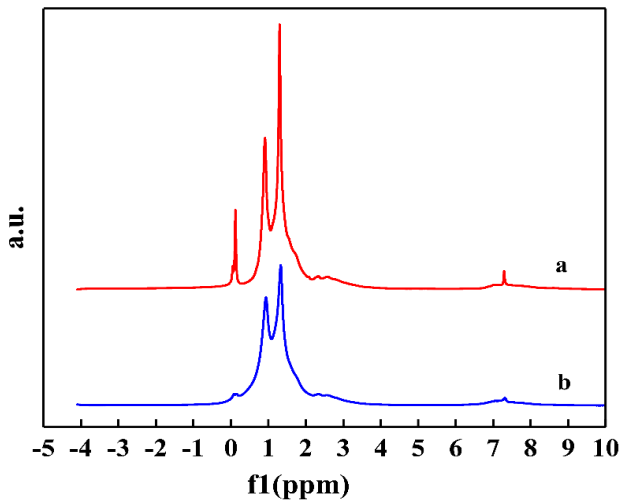

Figure 9 ^{1}H NMR Spectrum of (a) oil before reaction and (b) oil after aquathermolysis with the Fe_3O_4/ heulandite catalyst.

Table 6 Different parameters determined from ^{1}H NMR spectra.

Oil types	H_A (%)	H_α (%)	H_β (%)	H_γ (%)	Aromaticity condensation (H_{AU}/C_A)	Aromaticity (f_A)
Crude oil	0.06	0.11	0.48	0.19	0.252	0.539
Oil (Fe_3O_4/ heulandite)	0.03	0.10	0.58	0.27	0.223	0.447

Figure 9 shows the ^{1}H NMR spectrum of crude oil and oil after catalytic aquathermolysis with the catalyst. On the basis of the assignment of protons as shown in Table S1, two structural parameters, aromaticity (f_A) and aromaticity condensation

(H_{AU}/C_A) of oil before and after reaction can be calculated from formula 2 and 3:

The equation of aromaticity (f_A):

$$f_A = \frac{\frac{C_T}{H_T} - \left(H_\alpha + H_\beta + H_\gamma / 2H_T\right)}{C_T / H_T} \tag{2}$$

The equation of aromaticity condensation (H_{AU}/C_A):

$$\frac{H_{AU}}{C_A} = \frac{H_A / H_T + H_\alpha / 2H_T}{C_T / H_T - (H_\alpha + H_\beta + H_\gamma) / 2H_T} \tag{3}$$

In equations (2) and (3), H_A, H_α, H_β and H_γ can be calculated from Figure 9 according to Table S1. C_T and H_T represent total carbon and hydrogen respectively. The assignment of H atoms (i.e., H_A, H_α, H_β, H_γ) is listed in Table S1 and $H_T = H_A + H_\alpha + H_\beta + H_\gamma$. Two important structural parameters, aromaticity condensation (H_{AU}/C_A) and aromaticity (f_A) are shown in Table 6. After catalytic aquathermolysis with catalyst the aromaticity (f_A) of the oil decreased from 0.539 to 0.447 and the aromaticity condensation (H_{AU}/C_A) decreased from 0.252 to 0.223. The decrease of aromaticity (f_A) after reaction means that the amount of aromatic rings of the oil was reduced, which can be ascribed to two reasons. One is the opening and reconstruction of aromatic rings, and the other is the loss of macromolecules in the oil. The decrease of the aromaticity condensation (H_{AU}/C_A) demonstrates that some heavy molecules such as resin and asphaltene may have partly aggregated after catalytic aquathermolysis with the catalyst. The decrease of the aromaticity condensation (H_{AU}/C_A) can also be attributed to the breaking of the C-R bonds contained in the side chains, in accordance

with the result of elemental analysis. To sum up, the larger average pore diameter of Fe_3O_4 NPs can effectively reduce the S content of the crude oil by breaking C-S bonds, and by significantly decreasing the amount of heavy fractions (i.e., resin and asphaltene) (Figure 10). The easily prepared Fe_3O_4/heulandite with scalable preparation method remarkably decreased the oil viscosity by 85% in catalytic aquathermolysis, which is among the best heterogeneous catalyst for catalytic aquathermolysis of crude oil.

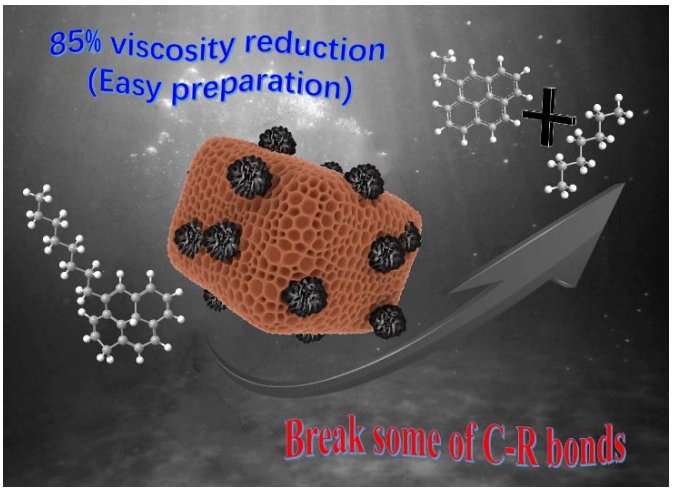

Figure 10 Schematic diagram of the good catalytic aquathermolysis performance over Fe_3O_4/heulandite catalyst.

4. Conclusions

In conclusion, the effect of Fe_3O_4 morphology in catalytic aquathermolysis of crude oil was first systematically studied. Two different Fe_3O_4 nanoparticles with different morphology were prepared by a co-precipitation method. It was found that the average pore diameter of the Fe_3O_4 was the determining factor. Larger average pore diameter makes more S-containing molecules contact active sites, which can effectively reduce the S content of the crude oil by breaking C-S bonds and by significantly

decreasing the amount of heavy fractions (i.e., resin and asphaltene). To further improve the effect of viscosity reduction, Fe_3O_4 nanoparticles were deposited on a natural zeolite to study the influence of catalyst in aquathermolysis. The Fe_3O_4/heulandite remarkably decreased the oil viscosity by 85% in catalytic aquathermolysis. The designed catalyst has the advantage of low-cost preparation with promising industrial application prospect. This has great potential for industrial exploitation of heavy oil.

Acknowledgments

This work was supported by the National Natural Science Foundation of China (21606254), the Key research and development plan of Shandong Province (2017GSF17126), the Independent innovation foundation of Qingdao (17-1-1-18-jch), and the Fundamental Research Funds for the Central Universities (18CX02014A).

References

[1] Maity S, Ancheyta J, Marroquín G. Catalytic aquathermolysis used for viscosity reduction of heavy crude oils: a review. Energy Fuels 2010;24(5):2809-16

[2] Muraza O, Galadima A. Aquathermolysis of heavy oil: A review and perspective on catalyst development. Fuel 2015;157:219-31

[3] Upreti SR, Lohi A, Kapadia RA, Elhaj R. Vapor Extraction of Heavy Oil and Bitumen: A Review. Energy Fuels 2007;21(3):1562-74

[4] Hein FJ. Heavy Oil and Oil (Tar) Sands in North America: An Overview & Summary of Contributions. Nat Resour Res 2006;15(2):67-84

[5] Chu Y, Fan C, Zhang Q, Zan C, Ma D, Jiang H, et al. The oxidation of heavy oil to enhance oil recovery: The numerical model and the criteria to describe the low and high temperature oxidation. Chem Eng J 2014;248:422-9

[6] Lin L, Zeng F, Gu Y. A circular solvent chamber model for simulating the VAPEX heavy oil recovery process. J Petrol Sci Eng 2014;118:27-39

[7] Wei LI, Zhu JH, Jian-Hua QI. Application of nano-nickel catalyst in the viscosity reduction of Liaohe extra-heavy oil by aquathermolysis. J Fuel Chem Technol 2007;35(2):176-80

[8] Chen Y, Wang Y, Lu J, Wu C. The viscosity reduction of nano-keggin-$K_3PMo_{12}O_{40}$ in catalytic aquathermolysis of heavy oil. Fuel 2009;88(8):1426-34

[9] Hyne J, Greidanus J, Tyrer J, Verona D, Rizek C, Clark P, et al. The Second International Conference on heavy crude and tar sands. Caracas, Venezuela 1982:25

[10] Clark PD, Dowling NI, Hyne JB, Lesage KL. The chemistry of organosulphur compound types occurring in heavy oils: 4. the high-temperature reaction of thiophene and tetrahydrothiophene with aqueous solutions of aluminium and first-row transition-metal cations. Fuel 1987;66(10):1353-7

[11] Clark PD, Dowling NI, Lesage KL, Hyne JB. Chemistry of organosulphur compound types occurring in heavy oil sands: 5. Reaction of thiophene and tetrahydrothiophene with aqueous group VIIIB metal species at high temperature. Fuel 1987;66(12):1699-702

[12] Clark PD, Hyne JB. Chemistry of organosulphur compound types occurring in heavy oil sands: 3. Reaction of thiophene and tetrahydrothiophene with vanadyl and nickel salts. Fuel 1984;63(12):1649-54

[13] Clark PD, Hyne JB, Tyrer JD. Chemistry of organosulphur compound types occurring in heavy oil sands:: 1. High temperature hydrolysis and thermolysis of tetrahydrothiophene in relation to steam stimulation processes. Fuel 1983;62(8):959-62

[14] Clark PD, Hyne JB, Tyrer JD. Some chemistry of organosulphur compound types occurring in heavy oil sands: 2. Influence of pH on the high temperature hydrolysis of tetrahydrothiophene and thiophene. Fuel 1984;63(1):125-8

[15] Wang Y, Chen Y, He J, Li P, Yang C. Mechanism of catalytic aquathermolysis: influences on heavy oil by two types of efficient catalytic ions: Fe^{3+} and Mo^{6+}. Energy Fuels 2010;24(3):1502-10

[16] Fan H-F, Liu Y-J, Zhong L-G. Studies on the synergetic effects of mineral and steam on the composition changes of heavy oils. Energy Fuels 2001;15(6):1475-9

[17] Fan H. The effects of reservoir minerals on the composition changes of heavy oil during steam stimulation. J Can Petrol Technol 2003;42(03)

[18] Yongjian L, Eryue C, Shoubin W. The Preparation and Evaluation of Oil-soluble Catalyst for Aquathermolysis of Heavy Oil [J]. Chem Eng Oil Gas 2005;6:019

[19] Chen Y, Wang Y, Wu C, Xia F. Laboratory experiments and field tests of an amphiphilic metallic chelate for catalytic aquathermolysis of heavy oil. Energy Fuels 2008;22(3):1502-8

[20] Chen Y, Yang C, Wang Y. Gemini catalyst for catalytic aquathermolysis of heavy oil. J Anal Appl Pyrol 2010;89(2):159-65

[21] FAN H-f, LI Z-b, Liang T. Experimental study on using ionic liquids to upgrade heavy oil. J Fuel Chem Technol 2007;35(1):32-5

[22] Hongfu F, Yongjian L, Liying Z, Xiaofei Z. The study on composition changes of heavy oils during steam stimulation processes. Fuel 2002;81(13):1733-8

[23] Fan H-f, Liu Y-j, Zhao X-f, Zhong L-g. Studies on effect of metal ions on aquathermolysis reaction of Liaohe heavy oils under steam treatment. J Fuel Chem Technol 2001;29(5):430-3

[24] Chuan W, Guang-Lun L, YAO C-j, SUN K-j, Gai P-y, CAO Y-b. Mechanism for reducing the viscosity of extra-heavy oil by aquathermolysis with an amphiphilic catalyst. J Fuel Chem Technol 2010;38(6):684-90

[25] Li J, Chen Y, Liu H, Wang P, Liu F. Influences on the aquathermolysis of heavy oil catalyzed by two different catalytic ions: Cu^{2+} and Fe^{3+}. Energy Fuels 2013;27(5):2555-62

[26] Nugraha MI, Noorlaily P, Abdullah M, Iskandar F. Synthesis of $Ni_xFe_{3-x}O_4$ Nanoparticles by Microwave-Assisted Coprecipitation and their Application in Viscosity Reduction of Heavy Oil. Mater Sci Forum 2013;737:204-8

[27] Nurhayati T, Iskandar F, Mikrajuddin A. Syntheses of hematite (α-Fe_2O_3) nanoparticles using

microwave-assisted calcination method. Mater Sci Forum 2013;737:197-203

[28] Lin D, Feng X, Wu Y, Ding B, Lu T, Liu Y, et al. Insights into the synergy between recyclable magnetic Fe_3O_4 and zeolite for catalytic aquathermolysis of heavy crude oil. Appl Surf Sci 2018

[29] Atacan K, Çakıroğlu B, Özacar M. Improvement of the stability and activity of immobilized trypsin on modified Fe3O4 magnetic nanoparticles for hydrolysis of bovine serum albumin and its application in the bovine milk. Food Chem 2016;212:460-8

[30] Ding C, Cheng W, Sun Y, Wang X. Novel fungus-Fe_3O_4 bio-nanocomposites as high performance adsorbents for the removal of radionuclides. J Hazard Mater 2015;295:127-37

[31] Joshi K, Rawat M, Gautam SK, Singh R, Ramola R, Singh F. Band gap widening and narrowing in Cu-doped ZnO thin films. J Alloy Compd 2016;680:252-8

[32] Ghosh R, Pradhan L, Devi YP, Meena S, Tewari R, Kumar A, et al. Induction heating studies of Fe_3O_4 magnetic nanoparticles capped with oleic acid and polyethylene glycol for hyperthermia. J Mater Chem 2011;21(35):13388-98

[33] Chao K, Chen Y, Li J, Zhang X, Dong B. Upgrading and visbreaking of super-heavy oil by catalytic aquathermolysis with aromatic sulfonic copper. Fuel Process Technol 2012;104:174-80

[34] Akrami H, Yardim M, Akar A, Ekinci E. FT-ir characterization of pitches derived from Avgamasya asphaltite and Raman-Dinçer heavy crude. Fuel 1997;76(14-15):1389-94

[35] Watson J, Jones D, Swannell R, Van Duin A. Formation of carboxylic acids during aerobic biodegradation of crude oil and evidence of microbial oxidation of hopanes. Org Geochem 2002;33(10):1153-69

[36] Nicodem DE, Guedes CL, Correa RJ. Photochemistry of petroleum: I. Systematic study of a Brazilian intermediate crude oil. Mar Chem 1998;63(1-2):93-104

[37] Colati KA, Dalmaschio GP, de Castro EV, Gomes AO, Vaz BG, Romão W. Monitoring the liquid/liquid extraction of naphthenic acids in brazilian crude oil using electrospray ionization FT-ICR mass spectrometry (ESI FT-ICR MS). Fuel 2013;108:647-55

[38] Faghihian H, Moayed M, Firooz A, Iravani M. Synthesis of a novel magnetic zeolite nanocomposite for removal of Cs^+ and Sr^{2+} from aqueous solution: Kinetic, equilibrium, and thermodynamic studies. J Colloid Interf Sci 2013;393:445-51

[39] Liu H, Peng S, Shu L, Chen T, Bao T, Frost RL. Magnetic zeolite NaA: Synthesis, characterization based on metakaolin and its application for the removal of Cu^{2+}, Pb^{2+}. Chemosphere 2013;91(11):1539-46

[40] Faghihian H, Moayed M, Firooz A, Iravani M. Evaluation of a new magnetic zeolite composite for removal of Cs^+ and Sr^{2+} from aqueous solutions: kinetic, equilibrium and thermodynamic studies. CR Chim 2014;17(2):108-17

[41] Deng Y, Qi D, Deng C, Zhang X, Zhao D. Superparamagnetic high-magnetization microspheres with an Fe_3O_4@ SiO_2 core and perpendicularly aligned mesoporous SiO_2 shell for removal of microcystins. J Am Chem Soc 2008;130(1):28-9

[42] Lee IS, Lee N, Park J, Kim BH, Yi Y-W, Kim T, et al. Ni/NiO core/shell nanoparticles for selective binding and magnetic separation of histidine-tagged proteins. J Am Chem Soc 2006;128(33):10658-9

[43] Daou T, Pourroy G, Bégin-Colin S, Greneche J, Ulhaq-Bouillet C, Legaré P, et al. Hydrothermal synthesis of monodisperse magnetite nanoparticles. Chem Mater 2006;18(18):4399-404

[44] Jiang W, Yang H-C, Yang S-Y, Horng H-E, Hung J, Chen Y, et al. Preparation and properties of

superparamagnetic nanoparticles with narrow size distribution and biocompatible. J Magn Magn Mater 2004;283(2-3):210-4